Mode-Specific Vibrational Reorganization Energies Accompanying Photoinduced Electron Transfer in the Hexamethylbenzene/Tetracyanoethylene Charge-Transfer Complex

Frances Markel,[‡] Nancy S. Ferris,[§] Ian R. Gould,[†] and Anne B. Myers*[,‡]

Contribution from the Center for Photoinduced Charge Transfer, University of Rochester, Rochester, New York 14627-0219, Department of Chemistry, University of Rochester, Rochester, New York 14627-0216, Eastman Kodak Company, Analytical Technology Division, Rochester, New York 14650-2132, and Eastman Kodak Company, Corporate Research Laboratories, Rochester, New York 14650-2109. *Received November 21, 1991*

Abstract: Resonance Raman excitation profiles have been measured across the broad, intense charge-transfer absorption band of the hexamethylbenzene/tetracyanoethylene complex in CCl_4 solution. Nonresonant Raman spectra of the complex and its perdeuterated derivative in the solid state have also been obtained with excitation at 1064 nm. Absorption of light within the charge-transfer band results in electron transfer from hexamethylbenzene to tetracyanoethylene to form a radical-ion pair. The geometry change along each vibrational mode as a result of this photoinduced electron transfer and the accompanying internal reorganization energies have been determined through quantitative simulation of the absorption spectrum and absolute resonance Raman intensities using time-dependent wavepacket propagation methods. The largest individual contributions to the total measured reorganization energy of approximately 3500 cm^{-1} arise from the presumed donor–acceptor intermolecular stretching mode at 165 cm^{-1} and the C=C stretch of tetracyanoethylene at 1551 cm^{-1}, with smaller contributions from other modes localized on both tetracyanoethylene and hexamethylbenzene. The importance of these results for understanding trends in the rates of nonphotochemical return electron transfer is discussed.

I. Introduction

Rates of electron-transfer reactions are often described by a Fermi Golden Rule expression, which is appropriate in the nonadiabatic (weak coupling) limit. The expression for the rate constant, k_{et}, is then usually written within the Born–Oppenheimer approximation as the product of an electronic matrix element squared, $|V|^2$, and a vibrational term which involves a thermally weighted sum of Franck–Condon factors, FC:

$$k_{et} = (4\pi^2/h)|V|^2\mathrm{FC} \qquad (1)$$

The matrix element V contains the dependence of the rate on the orientation of the reactants and their separation distance. The Franck–Condon factors contain the dependence on the density of states and total nuclear reorganization energy, λ. For electron transfer between molecules in solution, the Franck–Condon factors include contributions from both solvent motions, which are sufficiently low in frequency that they can be treated classically at most temperatures, and internal vibrations of the electron donor and acceptor, which usually must be handled quantum mechanically.[1-5] Therefore, in order to properly account for the quantum mechanical nature of the high frequency molecular vibrations, the frequencies and reorganization energies of these individual internal modes must be known.[6,7] Since such information is not generally available, the rates of electron-transfer reactions are usually described using models which employ a single "average" quantized vibrational mode with a frequency considered appropriate for the system of interest.[8-13] Often a value close to 1500 cm^{-1} is chosen for this averaged frequency, since this is close to the frequencies of skeletal stretching vibrations of aromatic systems. Clearly the assumption of a single high-frequency mode is at best a rough approximation, and the extent to which this approximation compromises the ability to extract from experimental rate data other parameters of interest, such as the solvent reorganization energy and the electronic coupling matrix element, is not generally clear. Furthermore, the usual assumption that skeletal stretching vibrations are the most important in electron-transfer reactions has been called into question by the recent observation of unexpected deuterium isotope effects which suggest that important contributions may arise from modes involving significant motion of donor methyl groups in aromatic radical cations.[14]

Evaluation of the contribution of high frequency intramolecular modes to the total reorganization energy requires knowledge of the frequencies of these vibrations in both the initial and final states, as well as the projection of the equilibrium geometry change between initial and final states onto each of these vibrational coordinates. Fischer and Van Duyne made a rather heroic attempt to obtain all the requisite parameters for the particular case of electron transfer from the radical anion of naphthalene to tetracyanoquinodimethane (TCNQ).[6] Their approach involved utilizing resonant and nonresonant Raman, infrared, and high resolution luminescence spectroscopies to obtain the vibrational frequencies of naphthalene, TCNQ, and their radical anions, estimating the geometry change for the naphthalene radical anion → naphthalene conversion from the Franck–Condon factors in the high resolution fluorescence spectrum, and obtaining the geometry change for the TCNQ → TCNQ radical anion conversion from the crystal structures of both species. In the end their analysis was only partially successful, and apparently most workers have since concluded that the effort involved in trying to work out the mode-specific reorganization energies is not worthwhile.

[‡] Department of Chemistry, University of Rochester.
[§] Eastman Kodak Co., Analytical Technology Division.
[†] Eastman Kodak Co., Corporate Research Laboratories.

(1) Buhks, E.; Bixon, M.; Jortner, J.; Navon, G. *J. Phys. Chem.* **1981**, *85*, 3759.
(2) Jortner, J. *J. Chem. Phys.* **1976**, *64*, 4860.
(3) Brunschwig, B. S.; Logan, J.; Newton, M. D.; Sutin, N. *J. Am. Chem. Soc.* **1980**, *102*, 5798.
(4) Siders, P.; Marcus, R. A. *J. Am. Chem. Soc.* **1981**, *103*, 741.
(5) Siders, P.; Marcus, R. A. *J. Am. Chem. Soc.* **1981**, *103*, 748.
(6) Fischer, S. F.; Van Duyne, R. P. *Chem. Phys.* **1977**, *26*, 9.
(7) Webman, I.; Kestner, N. R. *J. Chem. Phys.* **1982**, *77*, 2387.
(8) Miller, J. R.; Beitz, J. V.; Huddleston, R. K. *J. Am. Chem. Soc.* **1984**, *106*, 5057.
(9) Gould, I. R.; Ege, D.; Moser, J. E.; Farid, S. *J. Am. Chem. Soc.* **1990**, *112*, 4290.
(10) Liang, N.; Miller, J. R.; Closs, G. L. *J. Am. Chem. Soc.* **1990**, *112*, 5353.
(11) Murtaza, Z.; Zipp, A. P.; Worl, L. A.; Graff, D.; Jones, W. E., Jr.; Bates, W. D.; Meyer, T. J. *J. Am. Chem. Soc.* **1991**, *113*, 5113.
(12) Sigman, M. E.; Closs, G. L. *J. Phys. Chem.* **1991**, *95*, 5012.
(13) Franzen, S.; Goldstein, R. F.; Boxer, S. G. *J. Phys. Chem.* **1990**, *94*, 5135.
(14) Gould, I. R.; Farid, S. *J. Am. Chem. Soc.* **1988**, *110*, 7883.

0002-7863/92/1514-6208$03.00/0

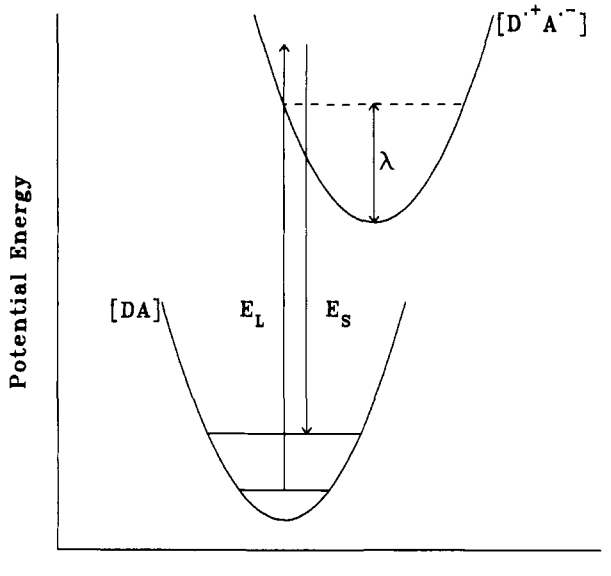

Figure 1. Potential energy surface diagram for Raman scattering on resonance with the charge-transfer band of a ground-state donor–acceptor complex. E_L and E_S are the energies of the exciting and scattered photons, respectively, and λ is the total electron-transfer reorganization energy. Since the energy difference between $D^{\bullet+}A^{\bullet-}$ and DA exceeds λ, the return electron-transfer reaction $D^{\bullet+}A^{\bullet-} \rightarrow$ DA is in the Marcus inverted region.

There is, however, a potentially easier way to obtain the internal reorganization energies of interest for the class of photoinduced charge-transfer reactions in which photoexcitation into a charge-transfer (CT) absorption band of the ground-state CT complex, DA, results in direct electron transfer to form a radical–ion pair, $D^{\bullet+}A^{\bullet-}$:

$$DA \xrightarrow{h\nu} D^{\bullet+}A^{\bullet-} \qquad (2)$$

In such systems the ground electronic state of the radical–ion pair is also the excited state of the neutral complex as illustrated in Figure 1. For the TCNE/HMB system the difference in energy between $D^{\bullet+}A^{\bullet-}$ and DA is larger than λ (vide infra), and thus the potential energy surfaces are "embedded". For this situation, the return electron-transfer reaction $D^{\bullet+}A^{\bullet-} \rightarrow$ DA is in the inverted region,[1-5] and may occur both nonradiatively and radiatively, although to our knowledge no charge-transfer emission spectra have yet been reported for this system. Importantly, since an electronic transition between the $D^{\bullet+}A^{\bullet-}$ and DA states corresponds to an electron-transfer process, the electron-transfer reorganization energies are simply related to the vibrational Franck–Condon factors for the electronic transition. The Franck–Condon factors could be extracted from the HMB/TCNE charge-transfer absorption spectrum alone if it were vibrationally structured. However, as is the case for essentially all DA systems in solution, the spectrum is featureless, and therefore the best way to deduce the underlying vibronic structure is through analysis of the resonance Raman scattering intensities.[15] Only those vibrations of the photoexcited system which are coupled to the electronic transition are resonantly enhanced in the Raman spectrum. The resonance Raman spectrum of a CT complex will therefore consist of those vibrations which are coupled to the DA $\rightarrow D^{\bullet+}A^{\bullet-}$ electron-transfer reaction. While quantitative analyses of resonance Raman intensities have previously been carried out on a variety of photoreactive molecules in solution phase, the utility of this method for probing electron-transfer reactions has remained relatively unappreciated. Thus far the most significant applications of resonance Raman intensity analysis to charge-transfer reactions are those of Hupp and co-workers, who have applied a simplified "short-time" version of Raman theory to infer mode-specific reorganization energies for a variety of charge-transfer transitions based on relative Raman intensities measured with pre- or post-resonance excitation.[16-22]

In this study we analyze the resonance Raman excitation profiles of the principal vibrational fundamentals, as well as intensities of several overtone and combination bands, to determine the vibrationally mode-specific internal reorganization energies accompanying photoinduced electron transfer in the D/A complex hexamethylbenzene/tetracyanoethylene (HMB/TCNE). Qualitative resonance Raman data for this complex have been in the literature for some time.[23-25] Here we present more complete experimental data, including absolute scattering cross sections, and determine the geometry changes accompanying photoinduced electron transfer by making use of modern theoretical methods for analysis of the absorption spectra and resonance Raman intensities.[15,26-30] Such an analysis has not been previously described for photoinduced electron-transfer processes. The ultimate goal of the present work is to obtain a common set of parameters describing the complex and its solvation properties which can be used to explain the rates of intermolecular electron transfer, the CT absorption and fluorescence spectra, and the resonance Raman spectrum, all of which depend in a similar manner upon the internal vibrational Franck–Condon factors and the solvation dynamics.

II. Experimental Methods

Tetracyanoethylene (Aldrich), hexamethylbenzene-d_{18} (MSD Isotopes), and spectroscopic grade CCl_4 (Eastman Kodak) and CH_2Cl_2 (Eastman Kodak) were used as received; hexamethylbenzene (Aldrich) was recrystallized several times from ethanol. Solutions in CCl_4 were made up at formal concentrations of approximately 6.7×10^{-4} M TCNE and 6.5×10^{-3} M HMB. A stoichiometric excess of the donor (HMB) was used because of the much higher solubility of HMB relative to TCNE, although this results in potential complications due to the formation of 2:1 (DAD) complexes.[25,31] According to the equilibrium constants determined by Liptay,[31] 1:1 complexes should outnumber 2:1 complexes by a factor of 20 or greater in all of our solutions. Our own measurements of absorbance as a function of concentration also indicate that we are working in a range where 2:1 complexes are unimportant. Unfortunately, these concentrations are lower than optimal for the resonance Raman studies, resulting in considerable spectral interference from the solvent Raman bands; therefore, spectra were also examined in CH_2Cl_2 to access regions of the spectrum hidden by CCl_4 bands. For the absolute Raman cross-section measurements, the complex concentrations were calculated from the maximum absorbance using the value of $\epsilon = 4613\ M^{-1}\ cm^{-1}$ for the 1:1 complex in CCl_4.[31]

Resonance Raman spectra were obtained using CW excitation from Ar^+ (Spectra-Physics 171-17), Kr^+ (Coherent Innova 90), and Ar^+-pumped dye lasers (Coherent CR-599). The incident light, at power levels ranging from 30 to 60 mW, was focused with a 7.5-cm f.l. lens onto a spinning cell containing a total volume of approximately 2 mL, and the Raman scattering was collected in a standard 90° geometry with the incident polarization perpendicular to the scattering plane. All experiments were carried out at ambient temperature (ca. 20 °C). Both po-

(15) Myers, A. B.; Mathies, R. A. In *Biological Applications of Raman Spectroscopy*; Spiro, T. G., Ed.; Wiley: New York, 1987; Vol. 2, p 1.

(16) Doorn, S. K.; Hupp, J. T. *J. Am. Chem. Soc.* **1989**, *111*, 1142.
(17) Doorn, S. K.; Hupp, J. T. *J. Am. Chem. Soc.* **1989**, *111*, 4704.
(18) Doorn, S. K.; Hupp, J. T.; Porterfield, D. R.; Campion, A.; Chase, D. B. *J. Am. Chem. Soc.* **1990**, *112*, 4999.
(19) Walker, G. C.; Barbara, P. F.; Doorn, S. K.; Dong, Y.; Hupp, J. T. *J. Phys. Chem.* **1991**, *95*, 5712.
(20) Blackbourn, R. L.; Johnson, C. S.; Hupp, J. T. *J. Am. Chem. Soc.* **1991**, *113*, 1060.
(21) Doorn, S. K.; Blackbourn, R. L.; Johnson, C. S.; Hupp, J. T. *Electrochim. Acta* **1991**, *36*, 1775.
(22) Blackbourn, R. L.; Johnson, C. S.; Hupp, J. T.; Bryant, M. A.; Sobocinski, R. L.; Pemberton, J. E. *J. Phys. Chem.* **1991**, *95*, 10535.
(23) Michaelian, K. H.; Rieckhoff, K. E.; Voigt, E.-M. *Proc. Natl. Acad. Sci. U.S.A.* **1975**, *72*, 4196.
(24) Jensen, P. W. *Chem. Phys. Lett.* **1977**, *45*, 415.
(25) Smith, M. L.; McHale, J. L. *J. Phys. Chem.* **1985**, *89*, 4002.
(26) Lee, S.-Y.; Heller, E. J. *J. Chem. Phys.* **1979**, *71*, 4777.
(27) Tannor, D. J.; Heller, E. J. *J. Chem. Phys.* **1982**, *77*, 202.
(28) Myers, A. B.; Mathies, R. A.; Tannor, D. J.; Heller, E. J. *J. Chem. Phys.* **1982**, *77*, 3857.
(29) Sue, J.; Yan, Y. J.; Mukamel, S. *J. Chem. Phys.* **1986**, *85*, 462.
(30) Yan, Y. J.; Mukamel, S. *J. Chem. Phys.* **1987**, *86*, 6085.
(31) Liptay, W.; Rehm, T.; Wehning, D.; Schanne, L.; Baumann, W.; Lang, W. *Z. Naturforsch. A* **1982**, *37A*, 1427.

larizations of scattered light were collected using reflective optics (off-axis ellipsoidal mirror) and passed through a quartz polarization scrambler before being imaged onto the entrance slit of a Spex 1877 0.6-m triple spectrograph. The detection system was a liquid nitrogen cooled CCD detector (Photometrics, Ltd). Spectral resolution was typically 4–8 cm^{-1} and signal was accumulated for 2–15 min at each setting of the spectrograph gratings. The Raman spectra indicated no decomposition of the sample during this time, and the intensities of the complex bands relative to solvent were independent of laser power over the range from 5 to 50 mW (at 568 nm). The spectra were corrected for the dependence of spectrograph throughput and detector sensitivity on detected wavelength by using a calibrated tungsten–halogen lamp (Optronics 220A). Reabsorption corrections were negligible (<5%) at all excitation frequencies based on the intensities of the CCl_4 solvent Raman bands in the absorbing solution relative to pure solvent. Integrated band intensities were obtained by using a nonlinear least-squares algorithm (Lab Calc, Galactic Industries) to fit regions of the spectrum to sums of Voigt profile peaks (mixed Gaussian/Lorentzian) plus a linearly sloping base line.

The quantity needed for comparison with theory is $\sigma_{R,i\rightarrow f}(E_L)$, the total Raman cross section for a particular $|i\rangle \rightarrow |f\rangle$ vibrational transition at incident laser photon energy E_L. The total scattered power (photons s^{-1}) resulting from the $|i\rangle \rightarrow |f\rangle$ transition, $P_{i\rightarrow f}(E_L)$, is given by

$$P_{i\rightarrow f}(E_L) = I(E_L)\sigma_{R,i\rightarrow f}(E_L) \quad (3)$$

where $I(E_L)$ is the incident intensity (photons cm^{-2} s^{-1}). Absolute Raman cross sections were measured relative to the CCl_4 doublet at 759 and 790 cm^{-1} as an internal standard as described, for example, in ref 15. The integrated absolute cross section of the CCl_4 doublet was determined by ratioing the CCl_4 band intensity to those of cyclohexane (802-cm^{-1} line)[32] and benzene (993-cm^{-1} line)[33] as external standards at excitation wavelengths of 458, 476, 482, 514, 530, 568, 607, 647, and 676 nm, using depolarization ratios of $\rho = 0.64$ for CCl_4 (measured at 530 nm), 0.06 for cyclohexane,[34] and 0.02 for benzene.[32,33] The cross sections obtained by using benzene as the standard were within 10% of those obtained using cyclohexane. The CCl_4 data were then fit to a standard "*A*-term" functional form[32,35] to allow interpolation between the measured points.

Crystals of the 1:1 complexes of HMB and HMB-d_{18} with TCNE were obtained by slow evaporation of a methylene chloride solution containing equimolar concentrations of the appropriate donor and acceptor. The needle-shaped crystals were mechanically extracted from the solids after evaporation. Normal (nonresonant) Raman spectra of the crystals were obtained on a Biorad/Digilab FTS40 FT–Raman system employing a Spectron SL301 CW Nd:YAG laser for excitation at 1064 nm. Detection over a wide spectral range was achieved by using a liquid nitrogen cooled germanium detector and dielectric filters that cut off 125 cm^{-1} from the laser line. Samples contained in 1-mm i.d. glass capillary tubes were excited with 500 mW of CW power, and the spectra were collected at 4-cm^{-1} resolution.

III. Method of Analysis

The objective of the data analysis is to determine the individual mode internal reorganization energies, λ, which depend on the displacements between the potential energy minima for the ground and excited electronic states along each mode. The experimental data consist of an absorption spectrum, resonance Raman excitation profiles (the absolute scattering intensity of a particular vibrational transition as a function of the laser excitation frequency) for the 14 strongest vibrations below 2300 cm^{-1} (omitting only the 450-cm^{-1} mode which is obscured by solvent scattering in CCl_4), and intensities for several higher frequency overtone and combination bands obtained with 514-nm excitation. These quantities depend on the potential energy surfaces for the ground and excited states. The challenge is to make use of the experimental data to reconstruct the true potential surfaces. However, there exists no *general* procedure for "inverting" the spectroscopic data to obtain the parameters of interest.

Accordingly, two approximate computational approaches for analyzing the absorption spectrum and resonance Raman intensity data were employed. Initial estimates of the geometry change along each Raman-active mode accompanying electronic excitation were made by using the "transform theory" analysis, which is based on the close similarity between the theoretical expressions for the optical absorption spectrum and the resonance Raman intensity.[15,36–38] These geometry changes were then refined through direct computation of the absorption spectra and Raman excitation profiles from "first principles" via the time-dependent wavepacket approach,[26–28,39,40] as modified to apply to molecules in the solution phase,[29,30,41] an approach which has previously been applied to a variety of large molecules.[15,42–46] The final values of the geometry changes, Δ, (in dimensionless coordinates) obtained from these calculations are related to the single mode internal reorganization energies, λ, as described below.

If the so-called "standard assumptions" hold (i.e., no coordinate dependence of the transition dipole moment, no inhomogeneous broadening, and harmonic vibrations), the resonance Raman excitation profile for each specific Raman fundamental can be calculated from the optical absorption spectrum via the transform theory as follows:

$$\sigma_{R,i\rightarrow f}(E_L) = \frac{E_L E_S^3 n^2 \Delta^2 (\langle n\rangle + 1)}{4\hbar^2 c^2 \pi^3} \left| A_o(E_L) - A_0(E_L - \hbar\omega)\right|^2 \quad (4)$$

where $\sigma_{R,i\rightarrow f}(E_L)$ is the Raman cross section at excitation energy E_L, E_S is the scattered photon energy, n is the solution refractive index, ω is the vibrational frequency, and Δ is the displacement in dimensionless normal coordinates between the potential minima of the ground and resonant electronic states along the vibrational mode of interest. The dimensionless coordinate, q, is related to the ordinary normal coordinate, Q, by $q = (\omega/\hbar)^{1/2}Q$; for example, for a stretching vibration the normal coordinate is defined as $Q = m^{1/2}r$, where r is the bond length and m the reduced mass, so $q = (m\omega/\hbar)^{1/2}r$. The dimensionless displacement, Δ, is related to the single mode reorganization energy, λ, by

$$\lambda = \hbar\omega\Delta^2/2 \quad (5)$$

The average thermal occupation number of the vibration at temperature T is given by $\langle n\rangle = [\exp(\hbar\omega/kT) - 1]^{-1}$, and A_0 is the Kramers–Kronig transform of the optical absorption spectrum, defined by[15,37]

$$A_0(E_L) = P\int_0^\infty \frac{\sigma_A(E)}{E(E - E_L)}\,dE + i\pi\frac{\sigma_A(E_L)}{E_L} \quad (6)$$

where $\sigma_A(E)$ is the absorption cross section at photon energy E. Thus the *band shape* of the Raman excitation profile (the intensity of a particular Raman transition as a function of the exciting laser frequency) is determined only by the absorption spectral band shape and that mode's vibrational frequency. The overall scaling factor needed to make the calculated and experimental profiles match gives the geometry change along that mode upon optical excitation. The corresponding expressions for overtone and combination band scattering are summarized in ref 15.

The transform theory method is easy to apply and is particularly useful for large molecules since it does not require explicit modeling of all the vibrational degrees of freedom. However, transform theory breaks down when the optical spectrum is significantly inhomogeneously broadened (due either to absorbers in different spectroscopic "sites" or to thermal excitation of Franck–Condon active modes) or when the dependence of the electronic transition moment on the nuclear coordinate is important. While the

(32) Trulson, M. O.; Mathies, R. A. *J. Chem. Phys.* **1986**, *84*, 2068.
(33) Schomacker, K. T.; Delaney, J. K.; Champion, P. M. *J. Chem. Phys.* **1986**, *85*, 4240.
(34) Myers, A. B.; Trulson, M. O.; Mathies, R. A. *J. Chem. Phys.* **1985**, *83*, 5000.
(35) Li, B.; Myers, A. B. *J. Phys. Chem.* **1990**, *94*, 4051.
(36) Cable, J. R.; Albrecht, A. C. *J. Chem. Phys.* **1986**, *84*, 1969.
(37) Page, J. B.; Tonks, D. L. *J. Chem. Phys.* **1981**, *75*, 5694.
(38) Stallard, B. R.; Champion, P. M.; Callis, P. R.; Albrecht, A. C. *J. Chem. Phys.* **1983**, *78*, 712.
(39) Heller, E. J.; Sundberg, R. L.; Tannor, D. *J. Phys. Chem.* **1982**, *86*, 1822.
(40) Heller, E. J. *Acc. Chem. Res.* **1981**, *14*, 368.
(41) Sue, J.; Mukamel, S.; Okamoto, H.; Hamaguchi, H.; Tasumi, M. *Chem. Phys. Lett.* **1987**, *134*, 87.
(42) Myers, A. B.; Harris, R. A.; Mathies, R. A. *J. Chem. Phys.* **1983**, *79*, 603.
(43) Myers, A. B.; Mathies, R. A. *J. Chem. Phys.* **1984**, *81*, 1552.
(44) Myers, A. B.; Trulson, M. O.; Pardoen, J. A.; Heeremans, C.; Lugtenburg, J.; Mathies, R. A. *J. Chem. Phys.* **1986**, *84*, 633.
(45) Ci, X.; Myers, A. B. *Chem. Phys. Lett.* **1989**, *158*, 263.
(46) Ci, X.; Pereira, M. A.; Myers, A. B. *J. Chem. Phys.* **1990**, *92*, 4708.

transform can be modified to treat these effects in approximate ways,[15,36,37,47-49] much of its simplicity is then lost. Furthermore, trial calculations in which we compared the simplest approximate transform with an "exact" treatment based on direct modeling indicated that the approximate method is not accurate enough to be useful when non-Condon effects (coordinate dependence of the transition moment) are important (see also ref 48).

We therefore used these excited-state geometry changes only as first approximations, which were then refined through direct modeling. The optical absorption spectrum is given by

$$\sigma_A(E_L) = \frac{4\pi e^2 E_L M_0^2}{3n\hbar^2 c}\sum_i P_i \int_{-\infty}^{\infty} d\delta\, G(\delta)\ \mathrm{Re}\int_0^{\infty} dt \langle \chi_i|\chi_i(t)\rangle \times \exp[i(E_L + \epsilon_i + \delta)t/\hbar]\exp[-g(t)] \quad (7)$$

where E_L is the incident photon energy, n is the solvent refractive index, P_i is the initial Boltzmann population of the $3N-6$ dimensional ground-state vibrational level $|i\rangle$ having energy ϵ_i above the zero-point, $G(\delta)$ is an inhomogeneous site distribution of electronic energies (usually assumed to be Gaussian), $|\chi_i\rangle = [M(q)/M_0]|i\rangle$ where $M(q)$ is the vibrational coordinate-dependent electronic transition length and M_0 is the transition length evaluated at the equilibrium nuclear configuration, and $|\chi_i(t)\rangle = e^{-iHt/\hbar}|\chi_i\rangle$ is this function propagated for time t on the excited-state potential surface; H is the excited state vibrational Hamiltonian. The transition moment μ is the transition length multiplied by the electron charge, e.

The function $\exp[-g(t)]$ represents the dynamic contribution of the solvent environment, treated as a frictionally overdamped oscillator:[50,51]

$$g(t) = g_R(t) + ig_I(t) \quad (8a)$$

with

$$g_R(t) = (D^2/\Lambda^2)[\exp(-\Lambda t/\hbar) - 1 + \Lambda t/\hbar] \quad (8b)$$

$$g_I(t) = (D^2/2kT\Lambda)[1 - \exp(-\Lambda t/\hbar)] \quad (8c)$$

Here D represents the strength of the coupling between the electronic transition and the solvation coordinate, while $\hbar/\Lambda$ gives the characteristic solvent time scale. The real part, $\exp[-g_R(t)]$, is a damping factor that interpolates smoothly from exponential in time (when $\Lambda \gg D$), giving a Lorentzian line shape of full width at half-maximum $2D^2/\Lambda$, to Gaussian in time (when $\Lambda \ll D$), giving a Gaussian line shape of standard deviation D (fwhm = $2.355D$). When a stochastic model of line broadening is used, where the solvent affects the chromophore but not vice versa, only the real part of $g(t)$ is obtained.[29] The imaginary part, $g_I(t)$, is obtained from the fluctuation–dissipation theorem and accounts for the effect of the chromophore on the solvent. This term is therefore responsible for solvation dynamics and the Stokes shift.[52,53] Close to the static limit ($\Lambda \ll D$), the imaginary part assumes the form

$$g_I(t) = (D^2/2kT)t/\hbar = \lambda_s t/\hbar \quad (9)$$

where λ_s is the solvent contribution to the reorganization energy.[50] As the best fits to our data were always obtained with $D \gg \Lambda$, we have employed eq 9 rather than the more general eq 8c in our calculations.

At the same level of approximation, the resonance Raman cross section is given by

$$\sigma_{R,i\to f}(E_L) = \frac{8\pi e^4 E_S^3 E_L M_0^4}{9\hbar^6 c^4}\int_{-\infty}^{\infty} d\delta\, G(\delta) \times \left|\int_0^{\infty} dt\, \langle \chi_f|\chi_i(t)\rangle \exp[i(E_L + \epsilon_i + \delta)t/\hbar]\exp[-g(t)]\right|^2 \quad (10)$$

where $|\chi_f\rangle = [M(q)/M_0]|f\rangle$, $|f\rangle$ being the final vibrational state in the Raman process.

For the purposes of these calculations, we assumed parallel ground- and excited-state normal modes (i.e., no Duschinsky effect), and expanded the coordinate dependence of the transition length only up to linear terms in the vibrational coordinates. Under these conditions, the multimode overlaps, $\langle \chi_f|\chi_i(t)\rangle$, factor into products of single-mode overlaps:[15,27]

$$\langle \chi_f|\chi_i(t)\rangle = \prod_j \langle \chi_f|\chi_i(t)\rangle_j \quad (11)$$

We further assumed equal ground- and excited-state vibrational frequencies in the calculations. Experimental frequencies are available for the TCNE radical anion,[54,55] and they differ from the ground-state frequencies by a maximum of 12%, an amount that was found in preliminary calculations to have little effect on the shapes of the best-fit excitation profiles or the reorganization energies. Expanding $M(q)$ as a Taylor series about the ground-state equilibrium geometry and discarding terms higher than linear in q leaves

$$\langle \chi_f|\chi_i(t)\rangle_j = \langle f|[1 + q_j(\partial M/\partial q_j)/M_0]\exp[-iHt/\hbar] \times [1 + q_j(\partial M/\partial q_j)/M_0]|i\rangle_j = \langle f|\exp[-iHt/\hbar]|i\rangle + [(\partial M/\partial q_j)/M_0] \times \{\langle f|q_j\exp[-iHt/\hbar]|i\rangle + \langle f|\exp[-iHt/\hbar]q_j|i\rangle\} \quad (12)$$

The first of the three terms in eq 11 is simply $\langle f|i(t)\rangle$, the overlap between the initial wave function propagated by the excited-state vibrational Hamiltonian and the final vibrational state, as discussed in detail elsewhere.[15,39,40] The two terms involving q can be simplified by writing q as a sum of raising and lowering operators, which converts the quantity in curly brackets into a linear combination of $\langle (f+1)|i(t)\rangle$, $\langle (f-1)|i(t)\rangle$, $\langle f|(i+1)(t)\rangle$, and $\langle f|(i-1)(t)\rangle$. The resulting time-dependent overlaps were then evaluated with analytic expressions given previously.[15,27,56]

It should be noted that our implementation of eqs 7 and 10 is exact within the harmonic approximation. In particular, we do not use the "short-time" approximations[39] that have been employed in previous Raman studies of photoinduced charge-transfer processes,[16,17,20-22] although for this system it turns out that the large homogeneous line width required to fit the data (vide infra) causes only very short-time dynamics to contribute to the absorption and Raman spectra.

The only Franck–Condon active vibration with a frequency below kT at room temperature is the 165-cm^{-1} mode. The thermal population in this mode was treated by evaluating the Boltzmann sum in eqs 7 and 10 through $n = 2$ in this mode, which accounts for 90% of the population. The sum $P_0 + P_1 + P_2$ was then normalized to unity.

IV. Results

Figure 2 shows the optical absorption spectrum of the HMB/TCNE complex and indicates the excitation wavelengths at which resonance Raman data were obtained. Figure 3 shows the resonance Raman spectra of the complex in CCl_4 excited at 514 nm, while Figure 4 compares the spectra of the complexes formed with protonated (h_{18}) and perdeuterated (d_{18}) HMB at 530 nm, near the absorption maximum. In Figure 5 is shown the HMB/TCNE spectrum in CH_2Cl_2 solvent obtained with excitation at 586 nm, revealing a fairly strong complex band at 450 cm^{-1} that is hidden under solvent bands in CCl_4. All of the labeled bands are resonance enhanced due to complex formation; at the concentrations employed, both TCNE alone and HMB alone give very weak spectra with their strongest bands weaker than by at least a factor of 10 than the strongest complex bands in Figures 3–5. Several qualitative conclusions are immediately evident from these spectra. First, while the strongest band in the complex spectrum is indeed close to the "traditional" frequency of 1500 cm^{-1}, there are several other reasonably strong bands at 165, 450,

(47) Stallard, B. R.; Callis, P. R.; Champion, P. M.; Albrecht, A. C. *J. Chem. Phys.* **1984**, *80*, 70.
(48) Chan, C. K. *J. Chem. Phys.* **1984**, *81*, 1614.
(49) Lu, H. M.; Page, J. B. *J. Chem. Phys.* **1988**, *88*, 3508.
(50) Bosma, W. B.; Yan, Y. J.; Mukamel, S. *Phys. Rev. A* **1990**, *42*, 6920.
(51) Mukamel, S. *Annu. Rev. Phys. Chem.* **1990**, *41*, 647.
(52) Loring, R. F.; Yan, Y. J.; Mukamel, S. *J. Chem. Phys.* **1987**, *87*, 5840.
(53) Yan, Y. J.; Mukamel, S. *J. Chem. Phys.* **1988**, *89*, 5160.
(54) Hinkel, J. J.; Devlin, J. P. *J. Chem. Phys.* **1973**, *58*, 4750.
(55) Jeanmaire, D. L.; Suchanski, M. R.; Van Duyne, R. P. *J. Am. Chem. Soc.* **1975**, *97*, 1699.
(56) Yan, Y. J.; Mukamel, S. *J. Chem. Phys.* **1986**, *85*, 5908.

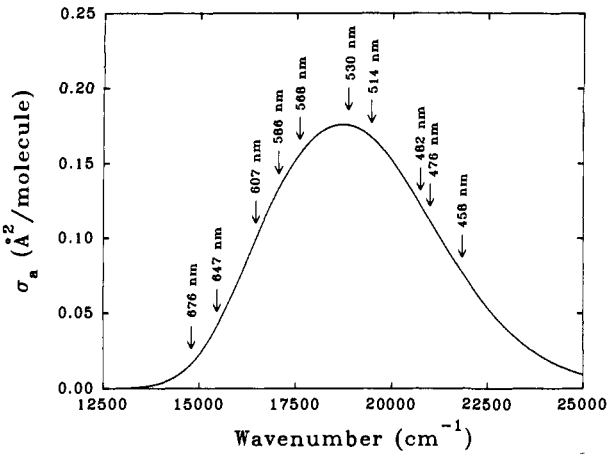

Figure 2. Optical absorption spectrum of the 1:1 HMB/TCNE complex in CCl_4 solution, indicating the excitation wavelengths at which resonance Raman spectra have been obtained. The absorption cross section σ_A, in units of Å^2/molecule, is related to the molar extinction coefficient ϵ, in units of L mol^{-1} cm^{-1}, by $\sigma_A = 2.303 \times 10^{19}\ \epsilon/N_A$ where N_A is Avogadro's number.

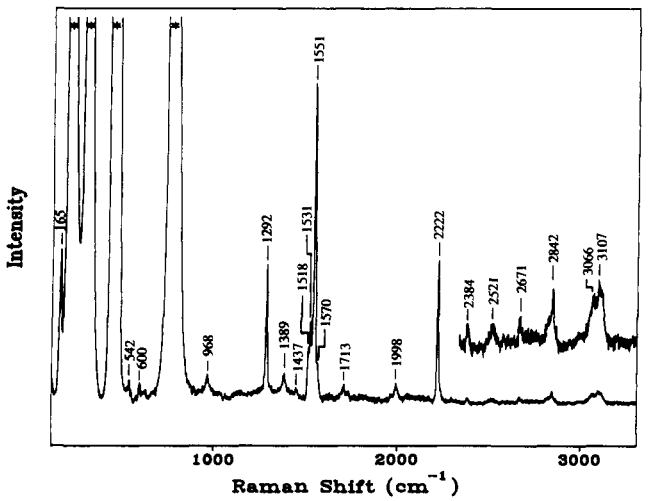

Figure 3. Resonance Raman spectrum of the HMB/TCNE complex in CCl_4 with excitation at 514 nm. Asterisks mark solvent bands. The inset is multiplied by a factor of 5.

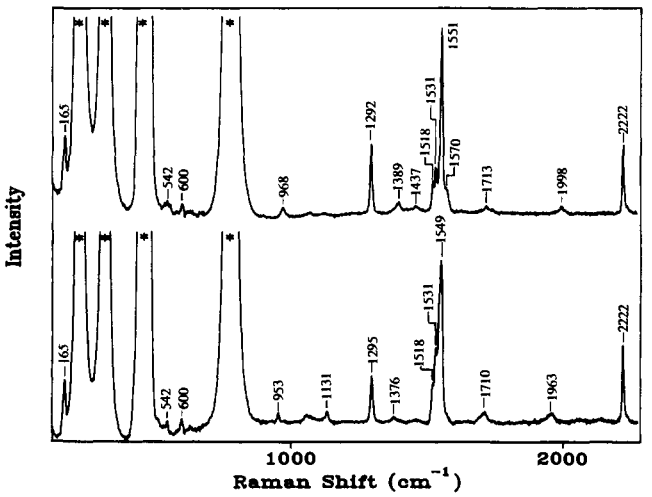

Figure 4. Resonance Raman spectra of HMB-h_{18}/TCNE (top) and HMB-d_{18}/TCNE (bottom) in CCl_4 with excitation at 530 nm. Asterisks mark solvent bands.

1292, and 2222 cm^{-1}, and many other weaker bands. Clearly a large number of vibrational modes spanning a wide range of frequencies are Franck–Condon active in the charge-transfer transition. Second, the relative intensities of the various Raman

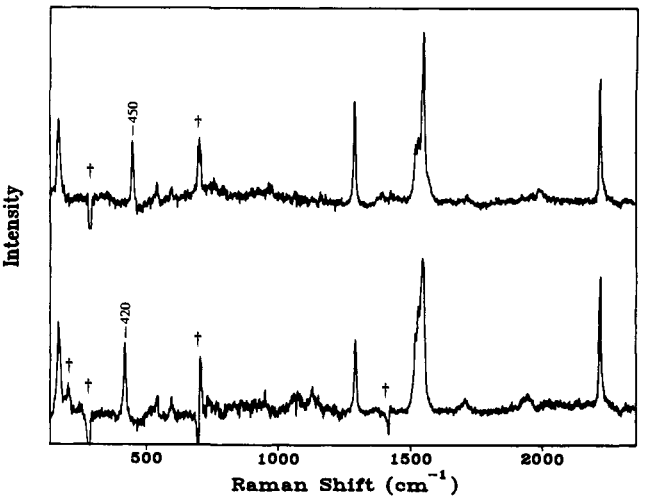

Figure 5. Resonance Raman spectra of HMB-h_{18}/TCNE (top) and HMB-d_{18}/TCNE (bottom) in CH_2Cl_2 with 586-nm excitation. Solvent bands have been subtracted; daggers mark residual solvent subtraction artifacts.

Table I. Resonance Enhanced Raman Bands of the HMB/TCNE Complex

frequency (cm^{-1})		rel int	
HMB-h_{18}	HMB-d_{18}	(514 nm)[a]	assignment[b]
165	165	177	D–A intermolecular str
450	420	59[c]	HMB (e_g C–CH_3 def)
542	542	6	ν_4 TCNE (a_g C–C≡N bend)
600	600	11	ν_3 TCNE (a_g C–C str)
968	953	33	HMB (e_g C–CH_3 str and CH_3 def)
1292	1295	100	HMB (a_{1g} C–CH_3 str and ring str)
1389	1376	39	HMB (a_{1g} CH_3 def)
1437	1131[d]	17	HMB (CH_3 antisym defs)
1518	1518	20	$\nu_{10} + \nu_{11}$ TCNE (b_{1u} C–C str + b_{1u} CN rock)
1531	1531	141	$\nu_{20} + \nu_{22}$ TCNE (b_{3g} C–C str + b_{3g} CN rock)
1551	1549	320	ν_2 TCNE (a_g C=C str)
1570		32	HMB (e_g ring str)
1713	1710	32	1551 + 165 comb band
1998	1963	35	1551 + 450 comb band
2222	2222	133	ν_1 TCNE (a_g C≡N str)
2384		11	2222 + 165 comb band
2521		23	1551 + 968 comb band
2671		9	2222 + 450 comb band
2842		36	1551 + 1292 comb band
3066		55	1551 + (1518,1531) comb band
3107		71	2 × 1551 overtone

[a] Integrated intensity (HMB-h_{18} complex) relative to that of 1292-cm^{-1} band, in CCl_4 solvent. [b] Assignments are based on refs 24, 54, 57–60. Symmetry labels are based on D_{2h} symmetry for TCNE and D_{3d} symmetry for HMB. [c] Intensity at 586 nm in CH_2Cl_2 (obscured by solvent in CCl_4). [d] Assignment of shifted frequency is uncertain.

lines are not strongly dependent on excitation wavelength (i.e., all modes have similar excitation profiles), suggesting that most of the resonance Raman enhancement derives from a single electronic transition. The observation by previous workers that the depolarization ratios for the stronger bands are all near 1/3 further supports this conclusion.[23-25] Third, most of the intense bands in the spectrum are only slightly, if at all, sensitive to perdeuteration of the donor, indicating that in this complex most of the Franck–Condon active modes (with the exception of the 1437- and, to a lesser extent, the 450-cm^{-1} modes) do not involve much motion of the HMB methyl hydrogens.

Table I summarizes the frequencies of the observed resonance enhanced modes, their isotopic shifts upon perdeuteration of the donor, their relative intensities with 514-nm excitation, and their vibrational mode assignments, which are in some cases still tentative. Although the analysis of our data to deduce the mode-

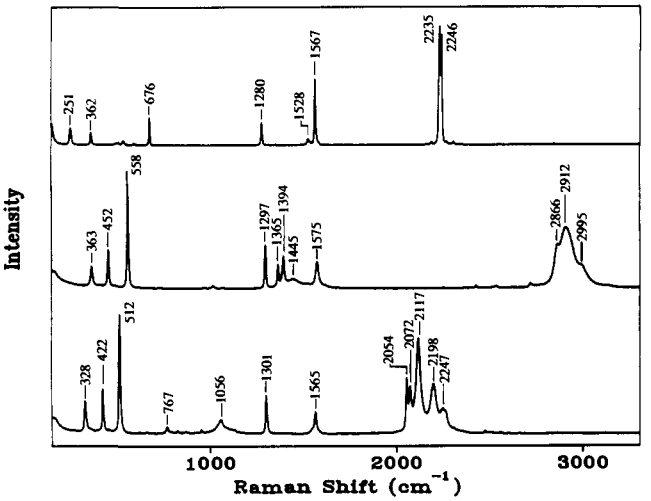

Figure 6. FT-Raman spectra of solid TCNE (top), HMB-h_{18} (middle), and HMB-d_{18} (bottom) with excitation at 1064 nm. Only the strongest bands are labeled.

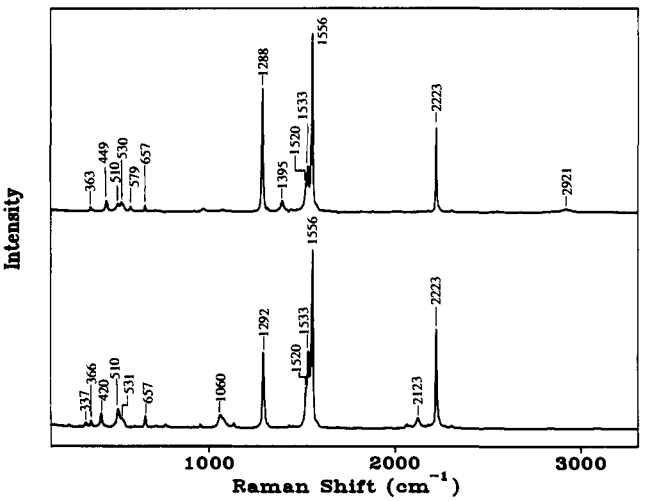

Figure 7. FT-Raman spectra of the 1:1 complexes of HMB-h_{18} with TCNE (top) and of HMB-d_{18} with TCNE (bottom), in the solid state with 1064-nm excitation. Only the strongest bands are labeled.

specific reorganization energies does not require knowledge of the normal mode assignments, it does require that we know whether the observed bands correspond to fundamentals, overtones, or combination bands, and so the question of the vibrational assignments must be addressed at this point. The clearest assignments are 2222 cm^{-1} and 1551 cm^{-1} as the totally symmetric C≡N stretch and the C=C stretch, respectively, of the complexed TCNE.[23,24,54,57] The bands at 600 and 542 cm^{-1}, which shift negligibly upon deuteration of HMB, are assigned as totally symmetric fundamentals of TCNE in agreement with ref 58. The two bands at 1518 and 1531 cm^{-1}, which also have no deuterium isotope shifts, are assigned as the totally symmetric combination bands of the TCNE CC stretching and CCN rocking fundamentals having b_{1u} and b_{3g} symmetry. Two bands in this region are also observed in our high resolution solid-state spectra of pure TCNE (Figure 6), while previous studies[24,57] detected only a single band in this region which was assigned as the combination band of the b_{3g} modes. The remaining lines below 2400 cm^{-1}, with the exception of the 165-cm^{-1} transition which we discuss below, all shift by at least 3 cm^{-1} upon deuteration and are therefore assigned as HMB modes or combination bands involving HMB modes, although some of the specific assignments must be considered tentative. The assignments of these bands are based on the published vibrational assignments of ref 59 together with our own FT-Raman spectra of solid HMB-h_{18} and -d_{18} (Figure 6), and are qualitatively reasonable based upon the isotopic shifts. Note that the 3-cm^{-1} upshift of the mode assigned as the a_{1g} methyl stretch at 1292 cm^{-1} can be explained by coupling of this mode with the methyl deformations, which shift from near 1400 cm^{-1} in HMB-h_{18} to near 1100 cm^{-1} in the d_{18} compound.

Figure 7 shows our nonresonant FT-Raman spectra of the solid-state 1:1 complexes of both HMB-h_{18} and -d_{18} with TCNE. To our knowledge these are the first nonresonant Raman spectra reported for this complex. The relative intensities are somewhat, though not drastically, different from those observed on resonance. The high resolution of these spectra allows us to clearly distinguish some bands that are strongly overlapped in the resonant spectra, and aids in making vibrational assignments. Table II summarizes the observed frequencies of the solid-state 1:1 complexes.

The assignment of the 165-cm^{-1} band has long been a subject of controversy. The many possibilities were recently discussed and analyzed in detail by McHale and Merriam.[60] In that publication they concluded that their earlier assignment[25] of this band to the first overtone of the donor-acceptor intermolecular stretch was correct, but they now prefer the assignment of this band to the fundamental of the intermolecular stretch.[61] The principal difficulty with this assignment of the 165-cm^{-1} band is the absence of any observable isotope shift. Treatment of the D-A stretch as a simple pseudodiatomic harmonic oscillator predicts a 4-cm^{-1} downshift upon perdeuteration of the donor. However, it is clear that both vibrational anharmonicities and mode mixing with other low-frequency vibrations will complicate the simple diatomic oscillator picture, and while TCNE itself has several vibrations in this general frequency region, attempting to assign the 165-cm^{-1} complex band to any one of them leads to difficulties as discussed in ref 60. The original assignment of this band as an overtone rather than a fundamental was based largely on the observation of a band at 89 cm^{-1} in the matrix-isolated infrared spectrum of the complex, which was assigned as the fundamental of the D-A stretch.[62] However, the resonance Raman spectra of large molecules with completely diffuse absorption spectra generally exhibit very little intensity in overtones, particularly overtones of very low-frequency modes, for reasons that are theoretically well understood.[15,39,42,43,63] It would be quite remarkable for an overtone of a mode below 100 cm^{-1} to have this much resonance Raman intensity under room-temperature solu-

Table II. Bands in Normal Raman Spectrum of HMB/TCNE Solid-State Complex Excited at 1064 nm[a]

frequency (cm^{-1})		frequency (cm^{-1})		frequency (cm^{-1})	
HMB-h_{18}	HMB-d_{18}	HMB-h_{18}	HMB-d_{18}	HMB-h_{18}	HMB-d_{18}
167 (w)	167 (w)	971 (w)	954 (w)	2003 (w)	
	246 (w)	1068 (w)	1060 (m)		2061 (w)
	337 (m)	1080 (w)	1079 (w)		2079 (w)
363 (m)	366 (m)		1133 (m)		2123 (m)
449 (m)	420 (m)	1288 (s)	1292 (s)	2147 (w)	
510 (m)	510 (m)	1317 (w)	1316 (w)	2178 (w)	2179 (w)
530 (m)	531 (m)	1395 (m)		2223 (s)	2223 (s)
579 (m)			1430 (w)	2230 (w)	
	599 (w)	1520 (m)	1520 (m)	2305 (w)	2306 (w)
657 (m)	657 (m)	1533 (s)	1533 (s)	2550 (w)	
711 (w)	713 (w)	1556 (s)	1556 (s)	2575 (w)	
	735 (w)	1582 (w)		2817 (w)	
	766 (w)		1693 (w)	2844 (w)	
895 (w)	880 (w)	1880 (w)		2921 (m)	
917 (w)	918 (w)			3107 (w)	3083 (w)

[a] s = strong, m = moderate, w = weak (qualitative intensities).

(57) Miller, F. A.; Sala, O.; Devlin, P.; Overend, J.; Lippert, E.; Lüder, W.; Moser, H.; Varchmin, J. *Spectrochim. Acta* **1964**, *20*, 1233.
(58) Michaelian, K. H.; Rieckhoff, K. E.; Voigt, E. M. *J. Mol. Spectrosc.* **1982**, *95*, 1.
(59) Bougeard, V. D.; Bleckmann, P.; Schrader, B. *Ber. Bunsenges. Phys. Chem.* **1973**, *77*, 1059.
(60) McHale, J. L.; Merriam, M. J. *J. Phys. Chem.* **1989**, *93*, 526.
(61) Britt, B. M.; Lueck, H. B.; McHale, J. L. *Chem. Phys. Lett.* **1992**, *190*, 6.
(62) Rossi, M.; Haselbach, E. *Helv. Chim. Acta* **1979**, *62*, 140.
(63) Schomacker, K. T.; Champion, P. M. *J. Chem. Phys.* **1986**, *84*, 5314.

Table III. Preliminary Dimensionless Displacements, Δ, for Vibrational Modes of HMB/TCNE Complex upon Photoinduced Electron Transfer Obtained from Transform Theory[a]

frequency (cm^{-1})	|Δ|	frequency (cm^{-1})	|Δ|	frequency (cm^{-1})	|Δ|
165	4.50	968	0.44	1437	0.23
450	1.31	1292	0.75	1551	1.06
542	0.57	1389	0.37	1570	0.31
600	0.56			2222	0.51

[a] Obtained by applying eq 4.

tion-phase conditions. More significantly, we have examined the resonance Raman spectrum down to about 50 cm^{-1} at several excitation wavelengths and see no indication of a band between 50 and 100 cm^{-1}. The D–A stretching fundamental is Raman allowed by symmetry, and while it is theoretically possible for an overtone to be much more intense than its fundamental (when most of the intensity derives from an excited-state frequency change rather than a change in equilibrium geometry), this is unlikely in the present case. We conclude that the 165-cm^{-1} band is a fundamental; whether it is really an intermolecular mode or a vibration localized on TCNE remains an open question.

With these tentative assignments in hand, we applied the transform theory as described in section III to obtain initial estimates of the excited-state displacement parameters for each of the 11 modes listed in Table I for which the Raman fundamentals were observed. With the assumptions employed (no vibrational coordinate dependence of the electronic transition moment and no changes in normal coordinates or vibrational frequencies between ground and excited states), the resonance Raman intensities arise entirely from the change in equilibrium geometry between ground and excited electronic states, and only totally symmetric complex modes can be resonance enhanced. (Note that the complex has lower symmetry than either monomer separately, and modes that are not totally symmetric in isolated TCNE or HMB can become resonance Raman allowed in the complex.) With this simplest set of assumptions, the shape of the Raman excitation profile for each fundamental is determined solely by the absorption spectrum and the mode frequency, and the multiplicative scaling factor needed to give the best fit between calculated and experimental absolute cross sections determines the excited-state geometry change in each mode (see eq 3). Our criterion for a "best fit" was that the sums of the experimental and calculated absolute intensities at the 10 excitation frequencies employed should match; this amounts, essentially, to fitting the integrated area of the Raman excitation profiles for the fundamentals. The profiles for the overtones and combination bands, including their absolute scaling, are then completely determined by these geometry changes and the absorption spectrum, providing a consistency check on the procedure. Table III lists the best-fit displacement parameters, Δ, and Table IV and Figure 8 compare representative experimental and calculated intensities. The

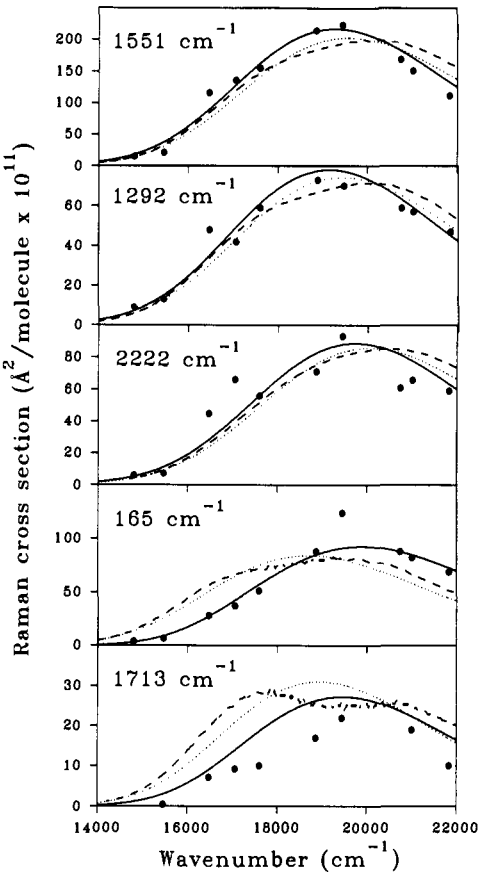

Figure 8. Experimental (solid circles) and calculated resonance Raman excitation profiles for the indicated Raman lines of the HMB/TCNE complex in CCl_4: dashed curve, transform theory calculation (Table III parameters); dotted curve, direct modeling without coordinate dependence of the transition moment (Table V parameters); solid curve, direct modeling with coordinate dependence of the transition moment (Table VI parameters). The assignments of the Raman lines are given in Table I. The noise in the transform calculated profiles for the 165- and 1713-cm^{-1} bands results from noise in the experimental absorption spectrum used as input for the transform and does not indicate real structure.

Table IV. Experimental and Calculated Raman Intensities at Two Wavelengths

	intensity (Å²/molecule × 10^{11})					
	514 nm			586 nm		
transition	expt	transform[a]	modeling[b]	expt	transform[a]	modeling[b]
165 fund	124	81	91	37	67	42
450 fund	–[c]			25[c]	26	26
542 fund	4.2	8.3	9.0	5.9	6.5	7.2
600 fund	7.7	9.7	12	5.9	7.5	9.4
968 fund	23	14	16	13	10	11
1292 fund	70	70	77	42	47	49
1389 fund	27	19	22	10	13	13
1437 fund	12	7.9	9.4	6.3	5.1	5.7
1551 fund	224	194	217	136	120	128
1570 fund	22	17	19	9.2	10	11
2222 fund	93	81	88	66	39	42
1551 + 165	22	26	27	9.2	25	8.6
1551 + 450	24	10	13	19	9.5	6.8
2222 + 165	7.7	11	10			
1551 + 968	16	4.4	6.2			
2222 + 450	6.3	4.4	5.0			
1551 + 1292	25	22	29			
2 × 1551	50	31	40			

[a] Calculated from parameters of Table III. [b] Calculated from parameters of Table VI. [c] Band obscured by solvent in CCl_4. Cross section at 586 nm estimated by ratioing to 1292-cm^{-1} band intensity in CH_2Cl_2 and scaling to measured absolute cross section of 1292-cm^{-1} band in CCl_4.

agreement between the experimental band shapes and those calculated using the transform approach for most of the fundamentals is fairly good, although in general the calculated profiles are broader than the experimental ones, particularly on the low-energy side of the absorption maximum. However, the fit to the 165-cm^{-1} fundamental band shape is particularly poor, and the calculated intensities for the two combination bands involving the 165-cm^{-1} mode are consistently too high. This indicates that the "standard assumptions" involved in the simple transform are not valid for this system, at least with respect to the 165-cm^{-1} mode.

It is well known that the relative intensities of overtones or combination bands relative to fundamentals depend strongly on the magnitude of the excited-state geometry changes; in fact, if the standard assumptions hold, overtone to fundamental ratios can be employed for determining the displacement parameters without any need for absolute intensity measurements.[36,64-66] If the transform calculation were overestimating *all* of the combination band and overtone intensities, that would suggest that the actual displacement parameters are all considerably smaller than those given in Table III, and that much of the breadth of the charge-transform absorption arises not from Franck–Condon activity in internal vibrations but from inhomogeneous broadening (different ground-state conformations or spectroscopically distinct solvation environments for different complexes). However, the observation that the transform predicts too much intensity only in combination bands involving the 165-cm^{-1} mode (while giving too little intensity in the other combination bands and overtones), together with the poor fit to the excitation profile band shape of the 165-cm^{-1} fundamental, suggests a more specific problem with this mode. Assuming this mode is the donor–acceptor stretch, the dependence of the electronic transition moment on vibrational coordinate should be significant,[67] and this is not considered by the simple transform theory employed here. The importance of such non-Condon effects was therefore explored by directly simulating the spectra via eqs 7–12. The parameters of Table III were taken as a starting point and were then adjusted by trial and error to optimize the simultaneous fit to the absorption spectrum and the resonance Raman intensities for all the observed lines. Note that there are four TCNE modes (ν_{10}, ν_{11}, ν_{20}, and ν_{22}) that appear only as combination bands and not as fundamentals or overtones, indicating (within the single resonant electronic state assumption) that these modes have neither significant displacements nor large frequency changes upon excitation, but undergo mode mixing (Duschinsky rotation) between ground and excited states. These were not included in our calculations, since modes that undergo only Duschinsky rotation upon excitation make no contribution to the reorganization energy and will contribute only slightly to the shape of the already extremely diffuse absorption spectrum.

Inclusion of nonzero dependence of the electronic transition length on the D–A stretching coordinate, with a concomitant decrease in the displacement parameter Δ in this mode, does indeed improve the calculated fits to the data. The intensities of combination bands involving this mode are somewhat reduced without reducing the intensity of the fundamental, and the excitation profile for the fundamental is considerably narrowed and blue-shifted, resulting in a much better fit to the experimental profile. The fit to the combination band intensities can be further improved by making $(\partial M/\partial q)$ larger and Δ smaller, but at the cost of a poorer fit to the shape of the profile for the fundamental. In order to obtain these results it is necessary to assume that Δ and $(\partial M/\partial q)$ are of opposite sign. (Note that the *overall* sign of both Δ and $(\partial M/\partial q)$ is irrelevant because the sign convention for the normal coordinate q is arbitrary; for pseudodiatomic stretching modes we take q to be positive as the bond length increases.) If they are assumed to have the same sign, the excitation profile for the fundamental becomes strongly red-shifted and in very poor agreement with the experimental profile. However, this result is difficult to rationalize physically, as discussed further in section V.

Table V. Preliminary Parameters for HMB/TCNE Complex Obtained from Direct Modeling without Coordinate Dependence of the Transition Moment[a]

freq (cm^{-1})	$\lvert\Delta\rvert$	freq (cm^{-1})	$\lvert\Delta\rvert$	freq (cm^{-1})	$\lvert\Delta\rvert$
165	4.70	968	0.44	1437	0.23
450	1.37	1292	0.74	1551	1.04
542	0.59	1389	0.36	1570	0.31
600	0.61			2222	0.50

[a] Other parameters [see eqs 7–10]: E_0 = 11 800 cm^{-1}, Λ = 110 cm^{-1}, D = 1100 cm^{-1}, no inhomogeneous broadening, M_0 = 0.87 Å.

Table VI. Final Reorganization Parameters for HMB/TCNE Complex from Direct Modeling with Coordinate Dependence of the Transition Moment[a]

freq (cm^{-1})	$(\partial M/\partial q)/M_0$[b]	Δ[c]	reorg energy (cm^{-1})	assignment[d]
165	0.07	−3.80	1191	D–A str
450	0.03	1.34	402	HMB
542	0.015	0.59	94	TCNE
600	0.02	0.61	112	TCNE
968	0.02	0.44	94	HMB
1292	0.045	0.73	344	HMB
1389	0.025	0.36	90	HMB
1437	0.015	0.23	38	HMB
1551	0.08	1.03	823	TCNE
1570	0.025	0.30	71	HMB
2222	0.055	0.48	256	TCNE

[a] Other parameters [see eqs 7–10]: E_0 = 11 600 cm^{-1}, Λ = 127 cm^{-1}, D = 1270 cm^{-1}, no inhomogeneous broadening, M_0 = 0.87 Å. [b] Derivative of electronic transition length with respect to vibrational coordinate, divided by transition length at ground-state equilibrium nuclear geometry. Signs are arbitrarily taken to be positive. [c] Displacement between equilibrium nuclear configuration of excited state ($D^{+}A^{-}$) and ground state (DA) in dimensionless normal coordinates. [d] See Table I for specific mode assignments.

While introducing dependence of the transition length on the D–A stretching coordinate significantly improves the calculated fits to the data, other discrepancies remain. In particular, most of the profiles for the higher frequency modes are calculated to be blue-shifted relative to the experimental ones. This suggests that there may be some coordinate dependence of the transition length along these modes as well; in order to red-shift the profiles, Δ and $(\partial M/\partial q)$ in these modes need to have the same, rather than different, signs. We hesitated, given the limited number of data points in our profiles, to introduce an additional freely adjustable parameter for each mode, feeling that the resulting best-fit parameters would be poorly defined. Instead, we derived a simple, approximate relationship between $(\partial M/\partial q)$ and Δ as outlined in the Appendix. The salient result is that for all modes other than the D–A stretch, $(\partial M/\partial q_j)$ is expected to be given by $K\omega_j\Delta_j$ where K is a positive coefficient. We thus have two free parameters, $(\partial M/\partial q)_{DA}$ and K, which define the dependence of the electronic transition moment on all the vibrational degrees of freedom.

Table V gives the best-fit parameters obtained from direct modeling without any coordinate dependence of the transition moment, while Table VI gives the parameters with $(\partial M/\partial q)$ included in all modes. Table IV shows the resonance Raman intensities at two excitation frequencies calculated from the full spectral modeling compared with those obtained from the simple transform and from experiment. Figure 8 compares the experimental excitation profiles for five representative transitions with the profiles calculated from the transform, from direct modeling without any coordinate dependence of the transition moment, and from the full modeling calculation, and Figure 9 compares the experimental absorption spectrum with that calculated from the full spectral modeling. Direct modeling without coordinate dependence of the transition moment does not give the same profiles as the transform because it involves only a finite number of

(64) Chinsky, L.; Laigle, A.; Peticolas, W. L.; Turpin, P.-Y. *J. Chem. Phys.* **1982**, *76*, 1.
(65) Brafman, O.; Chan, C. K.; Khodadoost, B.; Page, J. B.; Walker, C. T. *J. Chem. Phys.* **1984**, *80*, 5406.
(66) Gu, Y.; Champion, P. M. *Chem. Phys. Lett.* **1990**, *171*, 254.
(67) McHale, J.; Simons, J. *J. Chem. Phys.* **1979**, *70*, 4974.

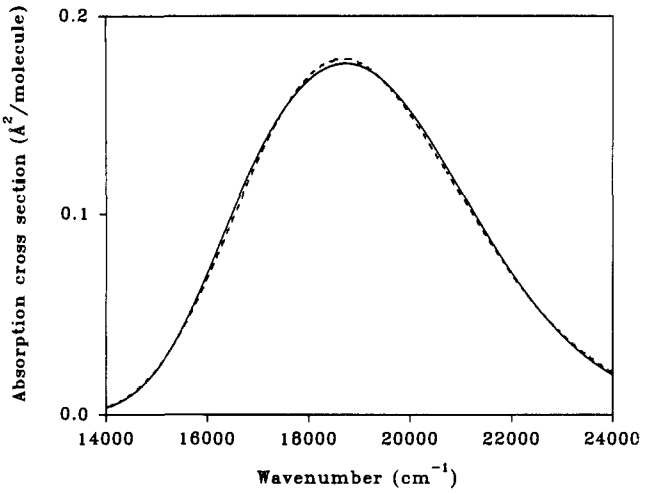

Figure 9. Experimental (solid) and final calculated (dashed) absorption spectra of HMB/TCNE in CCl_4. Parameters used in the calculation are given in Table VI.

harmonic modes and therefore cannot fit the absorption spectrum perfectly, whereas the transform implicitly contains an infinite number of modes (or, equivalently, a completely arbitrary line shape for each vibronic transition) as needed to reproduce the exact absorption spectrum. The absorption spectrum calculated without the coordinate dependence of the transition moment is not shown in Figure 9 for clarity, but it is very similar to that obtained from the full modeling calculation. Clearly the inclusion of nonzero $(\partial M/\partial q)$ improves the fits to the data, although for the 1551- and 2222-cm^{-1} modes the differences are slight.

V. Discussion

Our result that Δ and $(\partial M/\partial q)$ for the 165-cm^{-1} mode must be of opposite sign in order to fit the experimental excitation profile requires some further discussion. As the excited state certainly has a much greater degree of charge transfer than the ground state and will thus experience a greater Coulombic attraction between donor and acceptor, it appears reasonable that Δ in this mode be negative, that is, that the D–A equilibrium distance be smaller in the excited state than in the ground state. This then implies that $(\partial M/\partial q)$ must be positive, meaning that the magnitude of the transition dipole moment must increase as the donor–acceptor separation increases. This result is in agreement with the suggestion of McHale and Simons,[67] based on the simple approximation due to Mulliken[68] that the transition dipole moment should be directly proportional to the D–A distance, i.e., the distance through which the charge is transferred. That assumption, however, neglects the falloff of orbital overlap with increasing separation[69] and is clearly unreasonable at large D–A separations, where the transition moment must approach zero. PPP calculations on the HMB/TCNE complex predict the oscillator strength of the charge-transfer transition to decrease rapidly with increasing D–A separation in the vicinity of the ground-state equilibrium distance.[70] Experimentally most DA complexes show an increase in absorbance with pressure, although the HMB/TCNE complex behaves somewhat unusually; the dependence of absorbance on pressure for the complex in polymer matrices was found to be very small near 1 atm,[71] while for the complex both in CH_2Cl_2 solution[72] and in the solid state[73] the oscillator strength was found to first increase and then decrease with increasing pressure. While these pressure effect data do seem to imply an increase in transition moment with decreasing D–A separation, their interpretation is complicated because pressure changes many factors other than the donor–acceptor distance. Other experimental data are needed to evaluate the dependence of the transition moment on intermolecular separation. An attractive possibility would be to examine the complex of TCNE with a donor such as hexaethylbenzene, for which the steric hindrance imposed by the ethyl groups must force a significantly greater D–A separation than in the electronically very similar HMB; unfortunately, it was reported that no reliable values for the extinction coefficient of the CT band of hexaethylbenzene/TCNE could be obtained due to the weakness of the ground-state complex.[74] Finally, it should be noted that since the isotopic shifts indicate that the 165-cm^{-1} mode is not well described as a pure D–A stretch, the observation of a $(\partial M/\partial q)$ that seems physically unlikely for such a mode may not be surprising.

While the uncertainties in some of the mode assignments compromise our ability to obtain actual excited-state geometries from our data, the geometry changes that best fit our absolute resonance Raman intensities appear at least reasonable. The largest displacement in terms of dimensionless normal coordinates is $|\Delta| = 3.8$ in the 165-cm^{-1} mode, which we will continue to assign as the D–A stretch. For a stretching vibration, the dimensionless displacement Δ is related to the bond length change, δR, by $\delta R = (\hbar/m\omega)^{1/2}\Delta$, where m is the reduced mass and ω the vibrational frequency. Calculating the reduced mass as that of a pseudodiatomic D–A stretch gives a change of 0.21 Å in the donor–acceptor distance upon electron transfer. This distance is approximately 6% of the ground-state D–A equilibrium distance of 3.35 Å obtained from the X-ray structure of the solid HMB/TCNE complex.[75] (It is noteworthy that quantitative information concerning this mode cannot be obtained from even the most detailed spectroscopic data on the individual radical ions.) It should be pointed out, however, that we can obtain only a rough estimate of the excited-state D–A equilibrium separation because the actual excited-state frequency for the D–A stretch may differ significantly from that of the ground state. Resonance Raman intensities in low-frequency modes with large displacements depend mainly on the slope of the excited-state potential surface at the ground-state geometry.[39,42,43] Thus, if the D–A stretching frequency increases upon electronic excitation, the equilibrium geometry needed to generate the observed Raman intensity would become smaller than that obtained from our analysis, which assumes equal ground- and excited-state frequencies. The next largest displacement of $|\Delta| = 1.03$ in the C=C stretching mode of TCNE corresponds to a bond length change of 0.06 Å if the normal mode is taken to be an isolated CC stretch. This agrees well with the calculated bond length increase of 0.07 Å between neutral TCNE and its radical anion.[76]

Very recently McHale and co-workers have analyzed the resonance Raman excitation profiles of the HMB/TCNE complex in methylene chloride using transform theory to obtain excited-state geometry changes and non-Condon factors for the three strongest vibrations (168, 1550, and 2223 cm^{-1}).[61] The peak absorption cross section for the 1:1 complex is lower in CH_2Cl_2 than in CCl_4 by almost 40%, resulting in peak resonance Raman cross sections that are about a factor of 2 lower in methylene chloride. However, while the absorption spectra in the two solvents have very similar shapes, the excitation profiles measured by McHale's group for the 1550- and 2223-cm^{-1} modes in CH_2Cl_2 are considerably blue-shifted relative to those we obtain in CCl_4, leading to significantly different excited-state displacements and non-Condon factors for these modes. We find that the relative Raman intensities in CH_2Cl_2 and in CCl_4 with 586-nm excitation are very similar, but we have not attempted to measure full excitation profiles in methylene chloride, and cannot at present

(68) Mulliken, R. S. *J. Am. Chem. Soc.* **1952**, *74*, 811.
(69) Newton, M.; Sutin, N. *Annu. Rev. Phys. Chem.* **1984**, *35*, 437.
(70) Deperasińska, I. *Acta Phys. Pol.* **1975**, *A47*, 103.
(71) Offen, H. W.; Kadhim, A. H. *J. Chem. Phys.* **1966**, *45*, 269.
(72) Ewald, A. H. *Trans. Faraday Soc.* **1968**, *63*, 733.
(73) Jurgensen, C. W.; Peanasky, M. J.; Drickamer, H. G. *J. Chem. Phys.* **1985**, *83*, 6108.
(74) Frey, J. E.; Andrews, A. M.; Ankoviac, D. G.; Beaman, D. N.; Du Pont, L. E.; Elsner, T. E.; Lang, S. R.; Oosterbaan Zwart, M. A.; Seagle, R. E.; Torreano, L. A. *J. Org. Chem.* **1990**, *55*, 606.
(75) Saheki, M.; Yamada, H.; Yoshioka, H.; Nakatsu, K. *Acta Cryst.* **1976**, *B32*, 662.
(76) Lyons, L. E.; Palmer, L. D. *Aust. J. Chem.* **1976**, *29*, 1919.

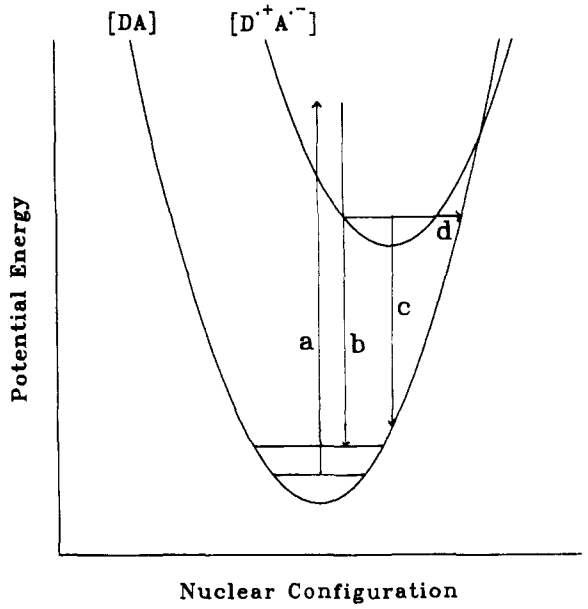

Figure 10. Potential energy surface diagram for ground-state donor–acceptor complex showing (a) charge-transfer absorption, (b) resonance Raman, (c) charge-transfer emission, and (d) nonradiative return electron-transfer processes.

explain why the profiles shown in ref 61 are so different from ours.

The total internal reorganization energy, λ_v, is approximately 3500 cm^{-1} (0.43 eV). This includes the contribution from the low-frequency D–A stretching mode, which would be considered to contribute to the solvent reorganization energy in the single frequency models. The sum of the reorganization energies of those modes which are localized on hexamethylbenzene is ca. 1040 cm^{-1}, and the corresponding sum for tetracyanoethylene is ca. 1280 cm^{-1} (Table VI). Together these localized reorganization energies would correspond to the total vibrational reorganization energy in the single frequency mode models, i.e., λ_v. The value obtained, ca. 0.29 eV, is very similar to that assumed previously for the closely related alkylbenzene/tetracyanoanthracene systems.[77] However, only about one-quarter of the total internal reorganization energy is due to modes with vibrational frequencies close to 1500 cm^{-1}. Importantly, no significant reorganization of the high frequency C–H stretching modes of the HMB is observed. This suggests that the deuterium isotope effects observed previously in the return electron-transfer reactions of the radical cation of this donor[14] are due not to changes in the methyl CH bond lengths upon electron transfer but to geometry changes along one of the lower frequency modes for which an effect of isotopic substitution is observed, perhaps the 450-cm^{-1} mode (Table I). It should be noted, however, that the resonance Raman intensities are sensitive to only that part of the potential energy surface of $D^{\cdot+}A^{\cdot-}$ which is close to the equilibrium geometry of DA, as indicated in Figure 10. The return electron-transfer process originates from the equilibrium geometry of $D^{\cdot+}A^{\cdot-}$ and yields the ground-state DA products in highly excited vibrational levels (Figure 10). If the potential energy surfaces are highly anharmonic, or if their shapes are strongly affected by solvent mode reorganization, then the Franck–Condon factors could be quite different for the different processes. In order to test whether the complete Franck–Condon analysis allows a quantitative understanding of the rates of return electron transfer, experimental rate data for the HMB/TCNE system would be required. Such data have not yet been reported for this specific system. In particular, it would be desirable to measure the effect of isotopic substitution on the rate of return electron transfer for $HMB^{\cdot+}/TCNE^{\cdot-}$ to compare with the isotope effects observed in the resonance Raman spectra. Estimates of the extent of electronic coupling in the HMB/TCNE and related radical–ion pairs are high,[73,77,78] which suggests that the weak coupling approximation might not apply for the return electron-transfer reactions.[77] Nevertheless, the Raman derived Franck–Condon data should still be directly applicable to the calculation of the return electron-transfer rate, unless it is controlled by other processes such as dynamical solvent effects.[77] A final test of the general applicability of the Raman data would be to fit the charge-transfer emission spectrum, although, as noted above, such a spectrum has not yet been reported for the HMB/TCNE system. The emission, like the return electron transfer, occurs from the equilibrium geometry of $D^{\cdot+}A^{\cdot-}$, but terminates in lower vibrational levels of the ground state (Figure 10). Thus the emission band shape, unlike the Raman intensities, is sensitive to that part of the excited-state potential surface near the ion-pair equilibrium geometry, but should be much less sensitive to ground-state vibrational anharmonicities than is the return electron transfer.

The solvent may in general contribute to the breadth of the optical transition through both "inhomogeneous" mechanisms (molecules that are spectroscopically distinct due to different solvation structures) and "homogeneous" mechanisms (broadening of each molecule's spectrum due to fast solvent fluctuations and solvent mode reorganization). We did not find it necessary to assume any inhomogeneous broadening in order to fit the data, but the fits are not very sensitive to this parameter; an inhomogeneous width of up to 1000 cm^{-1} or so could be accomodated without significantly affecting the quality of the fits. A moderate amount of solvent-induced *homogeneous* broadening is required to reproduce the experimental absolute Raman cross sections; the values of Λ and D (see eq 8) employed correspond to a nearly Gaussian homogeneous line shape having a full width at half-maximum of approximately 3000 cm^{-1}. Nevertheless, with the fitting parameters of Table VI most of the overall breadth of the absorption spectrum does arise from the underlying vibronic structure of the internal vibrations rather than from any solvent contribution (the solvent contribution is *convolved* with the width of the purely vibronic stick spectrum, not added to it), and the overtone and combination band intensities show that the displacement parameters employed in the calculated fits are reasonable.

In the model we have employed, all of the spectral breadth not due to the 11 internal modes listed in Table VI is attributed to a strongly overdamped, harmonic solvent mode of low frequency relative to kT, having a reorganization energy λ_s given by eq 9. Within this model λ_s is not an independent parameter but is determined uniquely by the values of the two damping parameters, Λ and D, which are adjusted to best fit the absolute Raman intensities and absorption band shape. The resulting value of λ_s = 3930 cm^{-1} (0.49 eV) appears far too large for a nonpolar solvent, and the value of E_0 = 11 600 cm^{-1} (1.44 eV) for the zero–zero energy of the CT electronic transition, which can be equated to the free energy for the intermolecular electron-transfer reaction,[79] seems correspondingly too low. It is likely that there are other contributions to the breadth (excited-state frequency changes and anharmonicities, internal vibrations not explicitly included, lifetime broadening of the vibronic transitions, etc.) which, if considered, would reduce λ_s. Errors in the absolute Raman intensities may also contribute to the excessively large value for λ_s obtained from our fits; if, for example, the absolute cross sections were 20–25% higher than measured (perhaps a reasonable upper limit on the uncertainty in our experimental cross sections), the data could be fit using a solvent-induced homogeneous line width about 40% smaller, with a resulting decrease of nearly a factor of 2 in λ_s. The fluorescence spectrum, when available, will be helpful in determining this parameter more accurately, as well as in exploring the possibility that more than one electronic transition contributes to the charge-transfer absorption band, as appears to be the case in some related complexes.[74] It is important to note, however, that although λ_s (via the homogeneous broadening) and E_0 are not determined accurately in the present study, the indeterminacy

(77) Gould, I. R.; Young, R. H.; Moody, R. E.; Farid, S. *J. Phys. Chem.* **1991**, *95*, 2068.

(78) Mulliken, R. S.; Person, W. B. *Molecular Complexes*; Wiley-Interscience: New York, 1969.

(79) Marcus, R. A. *J. Phys. Chem.* **1989**, *93*, 3078.

in these parameters does not significantly affect the values of the reorganization energies obtained for the Raman enhanced modes.

VI. Conclusions

Mode specific reorganization energies for the photoinduced electron-transfer reaction in the hexamethylbenzene/tetracyanoethylene CT complex have been obtained by modeling the excitation profiles of the resonance Raman bands of the complex. The inclusion of vibrational coordinate dependence of the electronic transition moment in the time-dependent wavepacket approach to modeling the data significantly improves the fits to the excitation profiles. The total vibrational reorganization energy of 0.43 eV is divided approximately evenly between modes which are localized on the hexamethylbenzene donor and those localized on the tetracyanoethylene acceptor, but the largest reorganization energy is associated with the presumed intermolecular D–A stretching mode at 165 cm^{-1}. The results presented here represent the most complete Franck–Condon data yet obtained for an intermolecular electron-transfer reaction. Work is in progress to use the Franck–Condon data to model the radiative and nonradiative return electron-transfer processes in the HMB/TCNE system.

Acknowledgment. The authors acknowledge Dr. Ralph Young and Professor Shaul Mukamel for enlightening discussions and for constructive comments on the manuscript. We also thank Professor Jeanne McHale for helpful discussions and for communicating results of her unpublished work. This work was supported through the NSF Science and Technology Center for Photoinduced Charge Transfer (CHE-88100264).

Appendix: Vibrational Coordinate Dependence of the Electronic Transition Moment

In Mulliken's theory of donor–acceptor charge-transfer complexes,[78] the ground and excited states of the complex, $|g\rangle$ and $|e\rangle$, are considered to be formed by mixing of the neutral or "no-bond" state, $|DA\rangle$, with the ionic state, $|D^+A^-\rangle$, through a coupling term in the total system Hamiltonian:

$$|g\rangle = a|DA\rangle + b|D^+A^-\rangle \quad \text{(A1a)}$$

$$|e\rangle = c|D^+A^-\rangle - d|DA\rangle \quad \text{(A1b)}$$

where a, b, c, and d are real positive constants whose magnitude depends on both the strength of the coupling, $\langle DA|H|D^+A^-\rangle$, and the energy separation δ between the basis states:

$$\delta = \langle D^+A^-|H|D^+A^-\rangle - \langle DA|H|DA\rangle = E_{D^+A^-} - E_{DA} \quad \text{(A2)}$$

Normally we expect $a \gg b$ and $c \gg d$. The overlap integral S is defined as

$$\langle DA|D^+A^-\rangle = S \quad \text{(A3)}$$

The true eigenstates must be normalized and orthogonal:

$$\langle g|g\rangle = 1 = a^2 + b^2 + 2abS \quad \text{(A4a)}$$

$$\langle e|e\rangle = 1 = c^2 + d^2 - 2cdS \quad \text{(A4b)}$$

$$\langle e|g\rangle = 0 = bc - ad + (ac - bd)S \quad \text{(A4c)}$$

The permanent dipole moments are given by

$$\langle g|\mu|g\rangle = \mu_g = a^2\mu_{DA} + b^2\mu_{D^+A^-} + 2ab\mu_{DA\rightarrow D^+A^-} \quad \text{(A5a)}$$

$$\langle e|\mu|e\rangle = \mu_e = c^2\mu_{D^+A^-} + d^2\mu_{DA} - 2cd\mu_{DA\rightarrow D^+A^-} \quad \text{(A5b)}$$

and the transition dipole moment for the charge-transfer transition is

$$\langle e|\mu|g\rangle = \mu_{g\rightarrow e} = bc\mu_{D^+A^-} - ad\mu_{DA} + (ac - bd)\mu_{DA\rightarrow D^+A^-} \quad \text{(A6)}$$

where μ_{DA} and $\mu_{D^+A^-}$ are the permanent dipole moments of the neutral and ionic basis states, and $\mu_{DA\rightarrow D^+A^-}$ is the transition dipole moment between these two states. We can neglect (bd) relative to (ac) in eq A6. Furthermore, since the permanent dipole moment of the fully ionic state should be much greater than that of the neutral state (in fact, μ_{DA} should not be exactly zero due to polarization effects,[80] but it should be small) and (bc) and (ad) should be of comparable magnitude, we can neglect the second term in eq A6. This leaves

$$\mu_{g\rightarrow e} = c(b\mu_{D^+A^-} + a\mu_{DA\rightarrow D^+A^-}) \quad \text{(A7)}$$

In general it is not clear that either term may be ignored. However, because $\mu_{D^+A^-} \gg \mu_{DA\rightarrow D^+A^-}$, $\mu_{g\rightarrow e}$ will increase as the amount of mixing between the basis states in the ground-state wave function is increased (b increases and a decreases). Thus it is usually considered that the oscillator strength of charge-transfer transitions arises from the degree of charge-transfer character in the ground electronic state. (The above analysis assumes $\mu_{g\rightarrow e}$ and $\mu_{D^+A^-}$ have the same direction, as found by Liptay for this complex.[31])

If we assume that it is only the energy gap, and not the strength of the coupling matrix element, that depends on vibrational coordinate, the dependence of the transition dipole moment on an arbitrary coordinate q_j may be expressed as

$$\partial\mu_{g\rightarrow e}/\partial q_j = (\partial\mu_{g\rightarrow e}/\partial\delta)(\partial\delta/\partial q_j) \quad \text{(A8)}$$

While this assumption is unlikely to be valid for the D–A stretch due to the dependence of the electronic coupling on intermolecular separation, it may not be a bad approximation for vibrations that are localized on the donor or acceptor. The first factor in eq A8 is independent of vibrational coordinate and simply refers to the change in transition moment as the energy gap between the neutral and ionic basis states is increased. Since increasing the energy gap will decrease the ground-state mixing and thereby decrease the transition moment, we conclude that $(\partial\mu_{g\rightarrow e}/\partial\delta)$ must be negative.

To evaluate the second factor, we assume that the potential energy curve for basis states $|DA\rangle$ and $|D^+A^-\rangle$, and for the eigenstates $|g\rangle$ and $|e\rangle$, are separable displaced harmonic oscillators having the same vibrational frequencies in all states, but different equilibrium geometries. Further, it makes sense that the geometries of $|g\rangle$ and $|e\rangle$ should be intermediate between those of $|DA\rangle$ and $|D^+A^-\rangle$, with $|g\rangle$ being closer in structure to the neutral state and $|e\rangle$ being closer to the ionic state. Hence we write the potential surfaces for the four states as follows:

$$V_{DA}(q) = \sum_i \hbar\omega_i q_i^2/2 \quad \text{(A9a)}$$

$$V_{D^+A^-}(q) = \sum_i \hbar\omega_i (q_i - \zeta_i)^2/2 \quad \text{(A9b)}$$

$$V_g(q) = \sum_i \hbar\omega_i (q_i - \epsilon\zeta_i)^2/2 \quad \text{(A9c)}$$

$$V_e(q) = \sum_i \hbar\omega_i (q_i - \gamma\zeta_i)^2/2 \quad \text{(A9d)}$$

where ζ_i is the shift in equilibrium geometry between the neutral and ionic basis states along normal coordinate q_i, and we expect $0 < \epsilon \ll \gamma < 1$. It is now straightforward to obtain the derivative,

$$(\partial\delta/\partial q_j) = -\hbar\omega_j\zeta_j \quad \text{(A10)}$$

Finally, the excited-state displacement Δ_j we obtain from our spectral modeling is the difference between the excited-state potential minimum (V_e) along mode j, given by $\gamma\zeta_j$, and the ground-state (V_g) minimum, given by $\epsilon\zeta_j$. Thus,

$$\Delta_j = (\gamma - \epsilon)\zeta_j \quad \text{(A11)}$$

and

$$(\partial\delta/\partial q_j) = -\hbar\omega_j\Delta_j/(\gamma - \epsilon) \quad \text{(A12)}$$

and since the denominator is positive, $(\partial\delta/\partial q_j)$ and Δ_j will be of opposite sign. Since $(\partial\mu_{g\rightarrow e}/\partial\delta)$ was found above to be negative, we conclude that $\partial\mu_{g\rightarrow e}/\partial q_j$ will be proportional to $\hbar\omega_j\Delta_j$ with the same, positive proportionality constant for all modes, as long as we accept the possibly dubious assumption that ϵ and γ in eqs A9 are mode-independent.

(80) LeFèvre, R. J. W.; Radford, D. V.; Stiles, P. J. *J. Chem. Soc. B* **1968**, 1297.

A qualitative explanation for this result is the following: starting from the ground-state equilibrium geometry, motion in the direction of Δ (toward the excited-state equilibrium geometry) reduces the energy gap between the neutral and ionic states, increasing their mixing and therefore increasing the magnitude of the transition moment. This result is expected to be qualitatively correct as long as the magnitude of the coupling between neutral and ionic basis states does not vary significantly with the vibrational coordinate of interest. It may not hold even qualitatively for the intermolecular donor–acceptor stretch due to the anticipated strong dependence of the coupling matrix element on donor–acceptor separation.

Molecular Geometry of Vanadyl–Adenine Nucleotide Complexes Determined by EPR, ENDOR, and Molecular Modeling[1a]

Devkumar Mustafi, Joshua Telser,[1b] and Marvin W. Makinen*

Contribution from the Department of Biochemistry and Molecular Biology, The University of Chicago, Cummings Life Science Center, 920 East 58th Street, Chicago, Illinois 60637.
Received December 23, 1991

Abstract: The interactions of the vanadyl ion (VO^{2+}) with the adenine nucleotides AMP, ADP, and ATP and the α,β-methylene analogue of ADP (AMP-CP) have been investigated by electron paramagnetic resonance (EPR) and electron nuclear double resonance (ENDOR) spectroscopy. By spectrometric titration of VO^{2+} in solutions of different VO^{2+}:nucleotide molar ratios near neutral pH, it was shown on the basis of the peak-to-peak amplitude of the −3/2 perpendicular EPR absorption feature that the stoichiometry of metal:ligand binding for ADP, AMP-CP, and ATP was 1:2. No evidence for the binding of AMP was observed. The proton ENDOR features of the $-CH_2-$ group of the terminal methylene-substituted pyrophosphate group in the $VO(AMP\text{-}CP)_2$ complex in 50:50 aqueous–methanol yielded electron–proton distances of 4.2 and 4.9 Å. This observation, together with the detection of ^{31}P superhyperfine coupling in EPR and ENDOR spectra, established that chelation of VO^{2+} occurs via the phosphate groups. Analysis of proton ENDOR features of $VO(ADP)_2$ and $VO(AMP\text{-}CP)_2$ complexes indicated the presence of only axially coordinated solvent in the inner coordination sphere with no equatorially bound solvent. Except for the absence of the $-CH_2-$ resonance features, the proton ENDOR spectrum of $VO(ADP)_2$ was identical with that of $VO(AMP\text{-}CP)_2$, including resonance features assigned to the nucleoside moiety, corresponding to electron–proton separations of 5.3 and 6.0 Å, respectively. The metal–proton resonances of the nucleoside moiety and of the two methylene protons of AMP-CP required that the two AMP-CP or ADP molecules bind to the vanadyl ion in a 2-fold symmetric manner in equatorial positions through the α and β phosphate oxygens. Only with the ENDOR determined metal–proton distances of 5.3 and 6.0 Å assigned to H(8) of the guanine base and to H(5′) of the ribose moiety, respectively, was a stereochemically acceptable conformation obtained by computer based torsion angle search calculations. The results of these calculations showed that (1) the orientation of the base with respect to the glycosidic C(1′)–N(9) bond was *anti*, (2) the conformation about the C(4′)–C(5′) bond was *gauche gauche*, and (3) the conformation about the C(5′)–O(5′) bond was *trans*. In $VO(ATP)_2$, proton ENDOR features characteristic of only axially bound water were observed, suggesting that the VO^{2+} was chelated via the terminal β and γ phosphate groups. The EPR and ENDOR results indicate that with all three nucleotides only [$VO(nucleotide)_2^{eq}(solvent)^{ax}$] species were formed.

Introduction

The interactions of nucleotides in biological systems, particularly ADP[2] and ATP,[2] require a divalent metal ion as a cofactor whereby the phosphate moiety of the nucleotide chelates the metal ion. To understand these processes, it is important to know the detailed molecular structure and geometry of metal–nucleotide complexes. However, the structures of only a few divalent metal complexes of ATP have been determined by X-ray crystallographic studies.[3] In the case of ADP, the only crystal structure that has been hitherto determined to atomic resolution is that of the monorubidium salt.[4] In solution, structures of metal–nucleotide complexes have been studied mainly by NMR methods.[5,6] In most NMR studies Mn^{2+} has been used as a paramagnetic ion to probe the conformation and binding of nucleotides in solution.[5a,c,6b] Structural data obtained by NMR methods depend primarily on measurements of the enhancement of the nuclear spin–lattice relaxation rate to estimate distances between magnetic nuclei and the paramagnetic metal ion. Since the relaxation rate is inversely proportional to the metal–nucleus distance raised to the sixth power, the NMR data are often not sensitive enough for precise assignment of the conformation of molecules in solution. Furthermore, from such NMR data it is often difficult to determine whether the resonance derives from a distinct conformer

(1) (a) This work was supported by a grant from the National Institutes of Health (GM 21900). (b) Postdoctoral trainee supported by a training grant from the National Institutes of Health (HL 7237). Present address: Department of Chemistry, Roosevelt University, 430 S. Michigan Avenue, Chicago, IL 60605.

(2) The following abbreviations are used: EPR, electron paramagnetic resonance; ENDOR, electron nuclear double resonance; hf, hyperfine; hfc, hyperfine coupling; rf, radiofrequency; PIPES, piperazine-*N*,*N*′-bis[2-ethanesulfonic acid]; AMP, adenosine 5′-monophosphate; ADP, adenosine 5′-diphosphate; ATP, adenosine 5′-triphosphate; AMP-CP, α,β-methyleneadenosine 5′-diphosphate; AMP-PCP, β,γ-methyleneadenosine 5′-triphosphate; AMP-CPP, α,β-methyleneadenosine 5′-triphosphate.

(3) (a) Kennard, O.; Isaacs, N. W.; Motherwell, W. D. S.; Coppola, J. C.; Wampler, D. L.; Larson, A. C.; Watson, D. G. *Proc. R. Soc. London, A* **1971**, *325*, 401–436. (b) Sabat, M.; Cini, R.; Haromy, T.; Sundaralingam, M. *Biochemistry* **1985**, *24*, 7827–7833. (c) Orioli, P.; Cini, R.; Donati, D.; Mangani, S. *J. Am. Chem. Soc.* **1981**, *103*, 4446–4452.

(4) Viswamitra, M. A.; Hosur, M. V.; Shakked, Z.; Kennard, O. *Nature* **1976**, *262*, 234–236.

(5) (a) Zetter, M. S.; Lo, G. Y.-S.; Dodgen, H. W.; Hunt, J. P. *J. Am. Chem. Soc.* **1978**, *100*, 4430–4436. (b) Bock, J. L. *J. Inorg. Biochem.* **1980**, *12*, 119–130. (c) Jarori, G. K.; Ray, B. D.; Rao, B. D. N. *Biochemistry* **1985**, *24*, 3487–3494.

(6) (a) Happe, J. A.; Morales, M. *J. Am. Chem. Soc.* **1966**, *88*, 2077–2078. (b) Cohn, M.; Hughes, T. R., Jr. *J. Biol. Chem.* **1962**, *237*, 176–181. (c) Tanswell, P.; Thornton, J. M.; Korda, A. V.; Williams, R. J. P. *Eur. J. Biochem.* **1975**, *57*, 135–145.

0002-7863/92/1514-6219$03.00/0